ON-LINE APPENDIX:

3D-TOF Acquisition Parameters

The FOV was $200 \times 200 \times 110$ mm^3 with a transverse orientation of the slabs. The acquisition and reconstruction voxel size were, respectively, $0.42 \times 0.73 \times 1.1$ mm^3 and $0.3 \times 0.3 \times 0.55$ mm^3. SENSE acceleration factor = 2.5, TR/TE = 25/3.5 ms, and flip angle = 20° yield an acquisition time of approximately 6 minutes.

4D-PCMR Acquisition Parameters

The FOV was $190 \times 210 \times 32$ mm^3. Acquisition and reconstruction voxel sizes were, respectively, 1 mm^3 isotropic and $0.8 \times 0.8 \times 1$ mm^3, with sensitivity encoding acceleration factor, 2; TR/TE, 4.6/2.9 ms; flip angle, 5°; and background phase error correction.[1] The sequence was triggered by the cardiac frequency using a peripheral pulse unit. The VENC was set to 80 cm/s by default, except for recent acquisitions in which the VENC was reduced to 40 cm/s after stent implantation to improve the low-velocity accuracy at the expense of aliasing artifacts. The positioning of the slices is illustrated in On-line Fig 1. For a heart rate of 65 beats per minute, the number of cardiac phases was 16, yielding an acquisition time of approximately 13 minutes.

Postprocessing

We combined the 4D-PCMR velocities with the vessel geometric information provided by the 3DRA. The main steps of the workflow (On-line Fig 2) were implemented in Matlab R2016b (MathWorks) and are briefly described below (more details are available in Bouillot et al[2]):

A) Segmentation of the 3DRA dataset with a watershed-based algorithm.[3,4] Subsequently, the center line of the segmented vessel was computed in a manner similar to that in Bouillot et al[5] using the VMTK library[6] (www.vmtk.org).

B) Aliasing correction of the 4D-PCMR velocities to remove phase jumps occurring during systole.

C) Rigid coregistration of the segmented vessel and the 4D-PCMR data in order to keep only the relevant velocity information within the circulating volume.

D) Linear interpolation of the velocity field on a refined grid (grid size of approximately 0.1mm).

E) This refined grid together with the surface nodes of the segmented vessel wall were used to compute a Delaunay tetrahedralization of the circulating volume (zero velocities were assumed at the vessel wall). The velocity field described on this tetrahedron mesh served as input data for further quantitative and qualitative analysis and were exported as a VTK file (The Visualization Toolkit; https://vtk.org).

Geometric Parameters and Flow Diversion

In parallel, aneurysm geometric parameters, such as volume, maximum diameter, aspect ratio, and neck size, were measured manually from 3DRA datasets as in Larrabide et al.[7] Potential relationships between these geometric parameters and PVRRs were investigated by means of a linear fit.

The average volume and maximum diameter of the 23 aneurysms were 378.6 mm^3 (range, 40–1656 mm^3) and 9.4 mm (range, 4.4–17.7 mm), respectively. The average aspect ratio and neck size were 1.32 (range, 0.69–2.32) and 5.5 mm (range, 2.5–13 mm), respectively. No correlations were found between these geometric parameters and the PVRRs (On-line Fig 3; R^2 = 0.24, 0.27, 0.02, 0.06 for volume, maximum size, aspect ratio, and neck size, respectively). Furthermore, no correlation between aneurysm geometric parameters and occlusion outcomes were found (On-line Fig 3, red and blue dots).

FDS Brand and Flow Diversion

A Kruskal-Wallis test was performed to assess differences between PVRRs and the 3 FDS brands used in this study (PED, FRED, and Silk). We showed that there were no significant differences (P = .72) in flow reduction among the 3 different devices implanted in the 23 patients and that the PVRR values for each stent were spread within a close range (On-line Fig 4), meaning that the stent brand did not influence the flow-reduction effect in this study. We also compared the occlusion rate for each implanted device (On-line Table). Even if the PED seems to perform slightly better in inducing thrombosis, we have to consider the small number of FRED and Silk devices used in our cohort, which mitigates these results.

Time-Averaged Velocities and PVRR

We computed the time-averaged velocity along the cardiac cycle before and after treatment for each patient and searched for correlations between the time-averaged PVRR and the outcomes (On-line Fig 5). As for systolic velocities, the same reduction trend was observed (a wide range of time-averaged velocities before stent placement and converging toward a narrower range after flow diversion). Unlike systolic PVRR showing a trend among the 3 groups of different occlusion times (P = .08), no relationship was found between the time-averaged PVRR and the occlusion time (P = .46). This might be explained by the time-averaging of the data, which includes proportionally more low-velocity values (below the threshold of 7.7 cm/s), which will affect the PVRR calculation even more.

REFERENCES

1. Walker PG, Cranney GB, Scheidegger MB, et al. **Semiautomated method for noise reduction and background phase error correction in MR phase velocity data.** *J Magn Reson Imaging* 1993;3:521–30 CrossRef Medline
2. Bouillot P, Delattre BMA, Brina O, et al. **3D phase contrast MRI: partial volume correction for robust blood flow quantification in small intracranial vessels.** *Magn Reson Med* 2018;79:129–40 CrossRef Medline
3. Higgins WE, Ojard EJ. **Interactive morphological watershed analysis for 3D medical images.** *Comput Med Imaging Graph* 1993;17:387–95 Medline
4. Meyer F. **Topographic distance and watershed lines.** *Signal Process* 1994;38:113–25 CrossRef
5. Bouillot P, Brina O, Ouared R, et al. **Geometrical deployment for braided stent.** *Med Image Anal* 2016;30:85–94 CrossRef Medline
6. Antiga L, Piccinelli M, Botti L, et al. **An image-based modeling framework for patient-specific computational hemodynamics.** *Med Biol Eng Comput* 2008;46:1097–1112 CrossRef Medline
7. Larrabide I, Aguilar ML, Morales HG, et al. **Intra-aneurysmal pressure and flow changes induced by flow diverters: relation to aneurysm size and shape.** *AJNR Am J Neuroradiol* 2013;34:816–22 CrossRef Medline

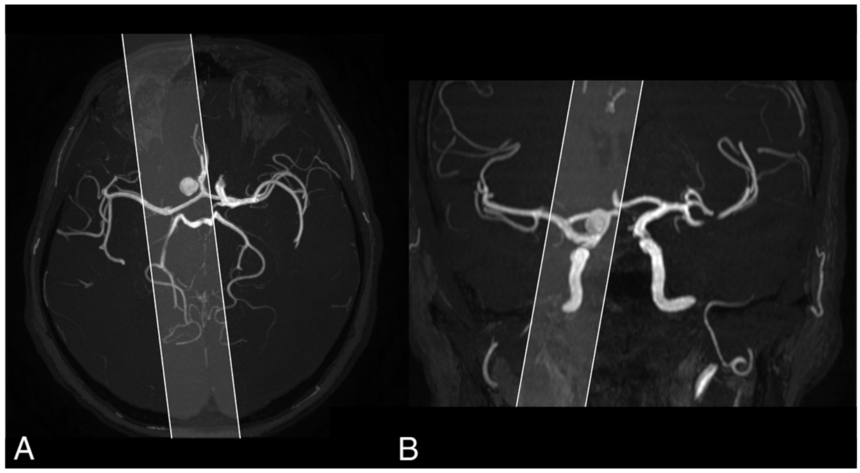

ON-LINE FIG 1. Typical MIP of the 3D-TOF (axial [*A*] and coronal [*B*] views) with the location of the 4D-PCMR slab (*white area*). Note the double obliquity of the sagittal slices required for complying with the 2 following constraints: 1) avoiding the nose, which is responsible for folding artifacts; and 2) covering the aneurysm bulge and the adjacent ICA.

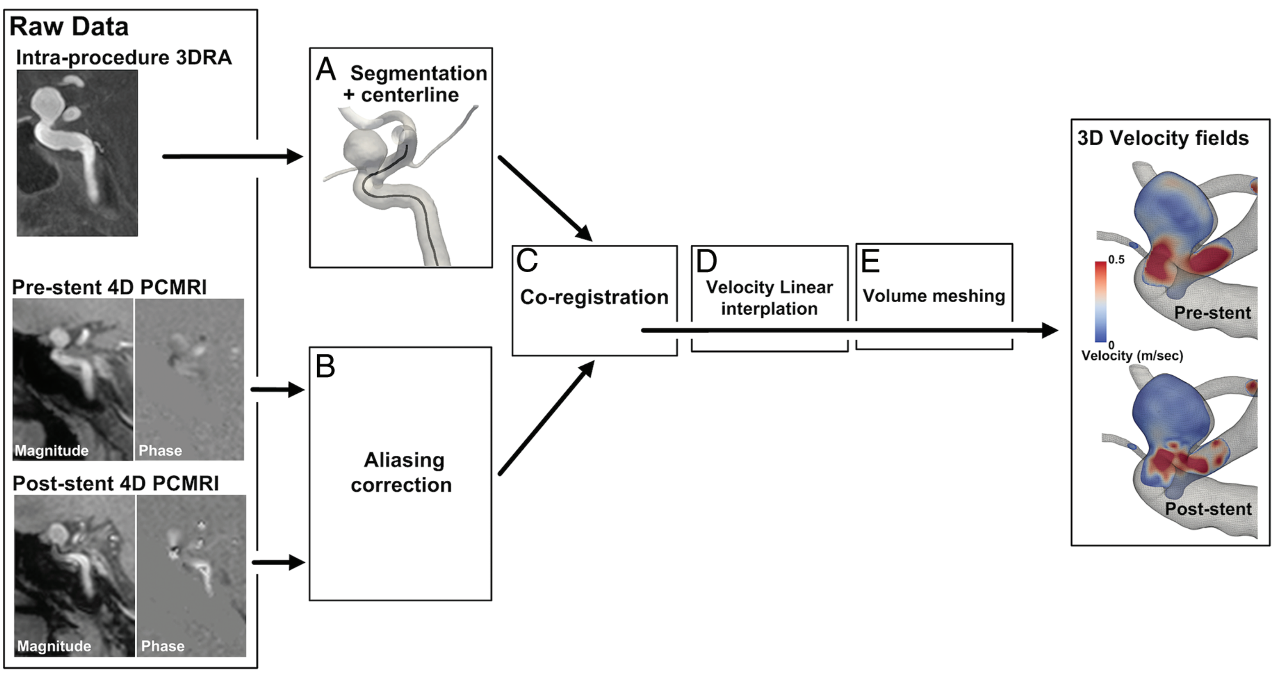

ON-LINE FIG 2. Velocity field construction from 4D-PCMR and 3DRA raw datasets. *A*, 3DRA vessel segmentation and center line. *B*, 4D-PCMR aliasing correction. *C*, Vessel geometry, 4D-PCMR coregistration. *D*, Velocity interpolation. *E*, Meshing of the circulating volume.

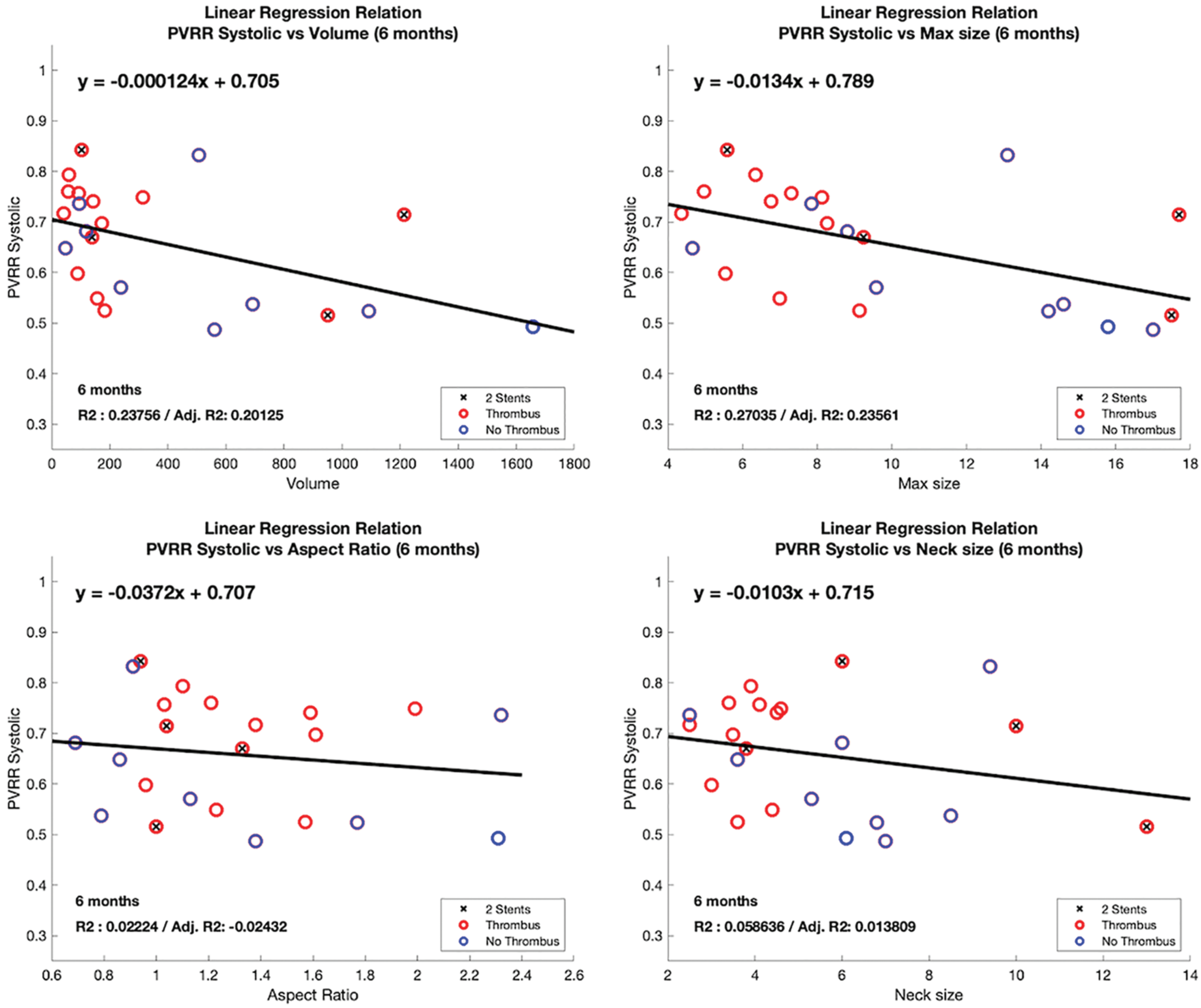

ON-LINE FIG 3. Linear regression between geometric parameters of the aneurysms (volume, maximum size, aspect ratio, and neck size) and flow reduction (PVRR). *Red and blue dots* represent occlusion and still circulating aneurysms at 6 months, respectively.

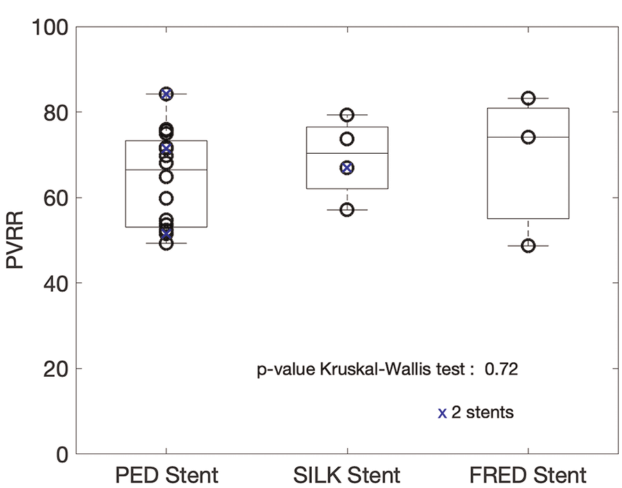

ON-LINE FIG 4. PVRRs for the 3 different FDSs used. *Blue cross dots* represent patients implanted with 2 stents.

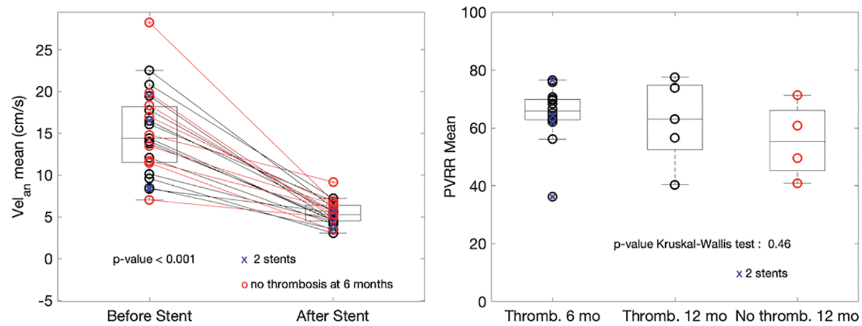

ON-LINE FIG 5. *Left*, Intra-aneurysmal time-averaged velocities along cardiac cycle before and after treatment. *Right*, Time-averaged PVRRs for patients thrombosed at 6 and 12 months and not thrombosed at 12 months. *Blue cross dots* represent patients implanted with 2 stents. Thromb indicates thrombosis.

On-line Table: Occlusion rates at 6 and 12 months for the 3 devices

Device	6-Month Occlusion	12-Month Occlusion	No Thrombosis at 12 Months
PED (16)	11 (69%)	14 (88%)	2 (13%)
Silk (4)	2 (50%)	3 (75%)	1 (25%)
FRED (3)	1 (33%)	2 (67%)	1 (33%)